

# Photoinduced optical retardation in mesostructured dye-doped films investigated by an imaging pump-probe technique

I.-G. Marino,<sup>1,\*</sup> D. Delmonte,<sup>1</sup> F. Pessini,<sup>1</sup> P. P. Lottici,<sup>1</sup> L. Cristofolini,<sup>1</sup> J. García-Macedo,<sup>2</sup> A. Franco,<sup>2</sup> and G. Valverde-Aguilar<sup>2</sup>

<sup>1</sup>*Dipartimento di Fisica, Università di Parma, Viale G. P. Usberti 7a, 43100 Parma, Italy*

<sup>2</sup>*Departamento de Estado Sólido, Instituto de Física, Universidad Nacional Autónoma de México, México D.F. C.P. 04510*

\*Corresponding author: [iari-gabriel.marino@fis.unipr.it](mailto:iari-gabriel.marino@fis.unipr.it)

Received September 8, 2008; revised December 4, 2008; accepted December 15, 2008;  
posted December 16, 2008 (Doc. ID 101358); published February 4, 2009

The photoinduced optical retardation in mesostructured polymeric materials containing photo-orientable dyes has been investigated as a function of time and pump irradiance by an imaging pump-probe technique. The mesostructured samples show higher maximum retardation and lower residual anisotropy than amorphous ones. Several hypotheses are made to explain both results, taking into account the influence of the mesostructures on the chromophores. The retardation-irradiance curves measured in different samples are fitted against current available models. © 2009 Optical Society of America

OCIS codes: 110.5405, 160.1190, 160.2900, 160.4236, 160.5335, 260.1440.

## 1. INTRODUCTION

Polymeric materials containing photoisomerizable azo-dye molecules become birefringent when illuminated with polarized light of a suitable wavelength and find wide applications for optical storage [1,2], optical switching [3,4], and surface-relief gratings [5–7]. Photoisomerization occurs when the azo-dye molecules are promoted from the lower-energy trans form to their cis form upon absorbing light. The process is angularly selective as the absorption probability is proportional to  $I \cos^2 \theta$ , where  $I$  is the pump irradiance on the film (power on unit area) and  $\theta$  is the angle between the molecular axis and the polarization of the incoming light. The cis form rapidly decays to trans, with a random orientation, and then it can absorb again. Under irradiation, each molecule undergoes several trans-cis-trans cycles. If the molecule decays to trans with its axis perpendicular to the light polarization, an equilibrium position is attained and reorientation will not take place anymore. Thus, the molecular distribution function becomes anisotropic and, as the polarizability of each single molecule is anisotropic also, birefringence and dichroism occur in the system. The birefringence ( $\Delta n$ ) can be revealed by measuring the transmission of a weak non-resonant probe beam through crossed polarizers in a pump-probe experiment [8].

In previous works [9,10], we applied a wide-field mapping technique to sol-gel derived photobirefringent systems. The wide-field mapping of the transmitted probe beam allows the measurement of the optical retardation  $\rho = \Delta n 2\pi d / \lambda$  (where  $d$  is the film thickness and  $\lambda$  is the probe wavelength) induced by a bell-shaped pump beam on an extended region of the sample and the determination of its dependence from the local pump irradiance ( $I$ )

and the irradiation time ( $t$ ). In this paper, we call this procedure the “imaging pump-probe (IPP) technique.”

Mesostructured polymeric or hybrid materials can be obtained by the insertion of surfactants into the starting solution [11,12]. In mesostructured photobirefringent systems, one can expect that the optical properties of the chromophore are highly sensitive to the local environment and that the mesostructures may have also indirect effects upon, for example, the chromophore–chromophore interactions. Indeed, it has been suggested that photoisomerizable dye molecules could be used to probe the internal structure of mesostructured systems [13], but the influence of the internal structure of mesostructured materials on the dynamics of their photoinduced properties is a field that still requires systematic investigations. In particular, it would be important to determine if the mesostructures have influence on the efficiency of the photoinduced birefringence (PIB) phenomenon and on the “memory” (residual birefringence) of the samples.

From a theoretical point of view, several models, obtained under different hypotheses, have been proposed to explain the kinetics of PIB in azo-dye-doped systems by Sekkat and Kroll [14], Sajti *et al.* [15], Thieghi *et al.* [16], and Fu *et al.* [17]. In these studies, the birefringence data are usually reported as time-dependent curves  $\rho(t)$  and the irradiance is taken as a parameter of the experiment. On the other hand, the IPP technique allows the measurement of continuous retardation-irradiance curves,  $\rho(I)$ , on which the models can now be directly tested.

Summarizing, in this paper we measure the photoinduced retardation of some dye-doped mesostructured polymeric films by our IPP technique, investigate the influence of mesostructures on the photoinduced properties,

and test the theoretical models on the retardation-irradiance curves. The dye molecules, Disperse Red 1 (DR1, 4-[*N*-ethyl-*N*-(2-hydroxyethyl)amino]-4'-nitroazobenzene) or Disperse Orange 3 (DO3, 4-(4-nitrophenylazo)aniline), are dispersed in a poly(methyl methacrylate) (PMMA) network (guest-host system). Cetyl trimethylammonium bromide (CTAB) and sodium dodecyl sulfate (SDS) have been used as templating agents. In the samples prepared with CTAB, one can expect that the dye molecules are located inside tubular cavities, which are arranged in a hexagonal mesostructure, while for the samples prepared with SDS the chromophores should lie between the planes of the lamellar mesostructure [11,12]. Visible absorption spectroscopy has been used to obtain additional information about the properties of the studied systems.

## 2. EXPERIMENTAL

Table 1 reports the sample list. DR1/PMMA thin films were synthesized by first dissolving DR1 (10 wt. %) and PMMA (90 wt. %) in tetrahydrofuran (THF) and stirring the solution for 20 min. The PMMA used has an average molecular weight ( $M_w$ ) of 120,000 g/mol. The molar ratio of the reagents in the starting solution was PMMA:DR1:THF=0.024:1:121. To prepare sample A2 (A3), 1.5 wt. % of CTAB (SDS) was added to the initial solution that then was stirred again for 5 min. Samples B1, B2, and B3 were obtained in a similar way, using DO3 instead of DR1.

All the solutions were filtered to remove undissolved particles and dust and then were dipcoated on glass substrates. Previous to the deposition of the films, the glass substrates were boiled in an acidic solution of sulphuric acid with hydrogen peroxide. The films were drawn with equipment that uses hydraulic motion to produce a steady and vibration-free withdrawal of the substrate from the sol [18]. Convection-free drying was critical to obtain high optical quality films.

Absorption spectra of the samples were collected with a double beam spectrophotometer Jasco model 7850 UV-Vis between 350 and 700 nm. The thickness was measured with a Thermomicroscope AutoProbe CP Research atomic force microscope (AFM) in noncontact mode; a small portion of the film was removed with a metallic blade and the profile was measured across the border of the removed region. The thickness of the films was about 2  $\mu\text{m}$ . In the IPP technique, the expanded and spatially filtered probe beam (632.8 nm, 10 mW, linearly polarized, nearly flat on

a 50 mm diameter) is transmitted through the sample and a crossed analyzer, and finally it is collected on a diffuser screen (Fig. 1).

The unexpanded pump beam (543 nm, 1 mW, linearly polarized at 45° with respect to the probe beam and slightly off axis) irradiates the sample inducing optical retardation. The fraction of the probe intensity transmitted by the analyzer depends on the local retardation of the sample, and its spatial distribution is mapped with a digital camera (computer controlled FireWire b/w DMK 41BF02 camera, equipped with a MeVis-C 16/1.6 lens) pointed to the diffuser screen. A long-pass optical filter prevents green light from reaching the screen.

To obtain a retardation map, we start by acquiring an image of light transmitted by the sample at crossed polarizers,  $I_{\perp}^T(x,y)$ . The analyzer is then rotated 90° by a computer-controller stepping motor and the image at parallel polarizers,  $I_{\parallel}^T(x,y)$ , is acquired. To reduce the CCD noise, each image is obtained as the average of 16 shots.  $I_{\parallel}^T(x,y)$  is used to normalize  $I_{\perp}^T(x,y)$  in order to eliminate the probe fluctuations in the calculation of the retardation map [9]

$$\rho(x,y) = 2 \arctan \sqrt{\frac{I_{\perp}^T(x,y)}{I_{\parallel}^T(x,y)}}.$$

With this setup, the spatial maps of the photoinduced retardation,  $\rho(x,y)$ , were acquired during a cycle of irradiation (pump on, 132 min= $t_{\text{MAX}}$ ) and relaxation (pump off, 268 min= $t_{\text{LAST}}$ ) with a time step of 2 min between each map. In addition, five maps of the unperturbed (isotropic) sample were recorded before starting irradiation for reference purposes. All the maps were downsized by a factor of 4 (original size: 1280  $\times$  960 pixels), and the spot area was cropped to remove the outer dark region, obtaining small maps formed by 40  $\times$  40 values, corresponding to a real size of about 2.3 mm  $\times$  2.3 mm.

At each time, the maps were correlated pixel-to-pixel to the pump irradiance map  $I(x,y)$  (which was acquired once before the measurement run). The correlation is obtained as follows: the  $I(x,y)$  matrix is transformed to a monodi-

**Table 1. List of the Samples with Chemical Components**

Name	Components
A1	PMMA:DR1
A2	PMMA:DR1:CTAB
A3	PMMA:DR1:SDS
B1	PMMA:DO3
B2	PMMA:DO3:CTAB
B3	PMMA:DO3:SDS

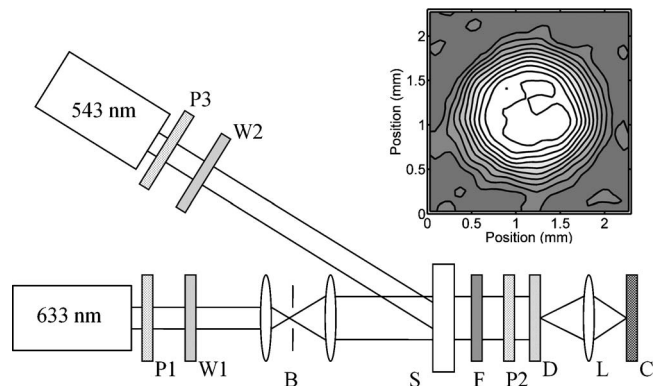


Fig. 1. IPP optical setup. Polarizers (P1 and P3) and half-wave plates (W1 and W2) for 632.8 and 543 nm are used to set the proper polarization of the probe and the pump beams. The probe beam passes through a beam expander with spatial filter (B). S, sample; F, long pass optical filter; P2, analyzer; D, diffuser screen; L, imaging lens; C, CCD camera. Inset, the bright circular region in the image (plot of level curves) is due to a PIB spot written in the sample A1.

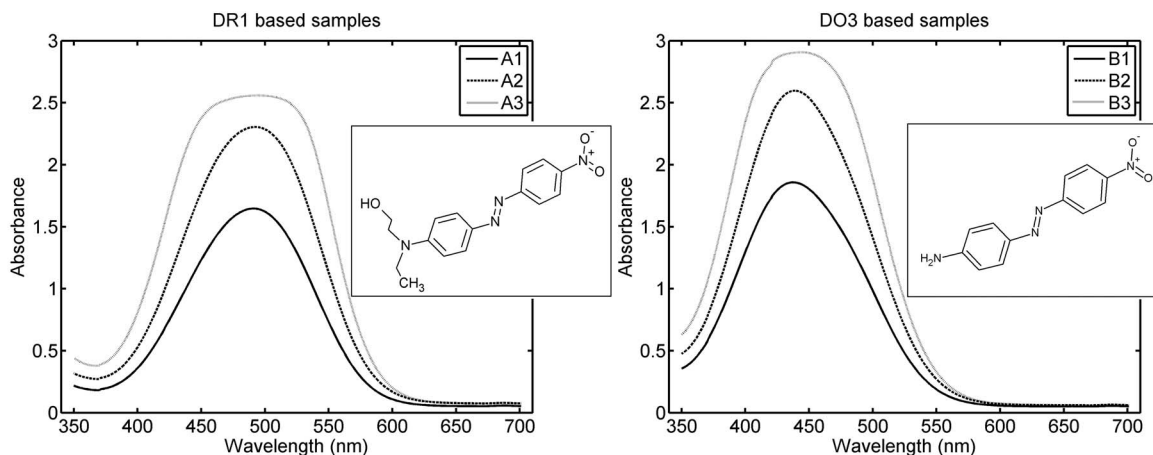


Fig. 2. Absorption spectra of the samples in the visible range. Left, DR1-based samples; inset, DR1 molecule. Right, DO3-based samples; inset, DO3 molecule. The flatness of the absorption band of samples A3 and B3 is not due to instrumental saturation.

mensional array and is sorted in ascending order; the  $\rho(x,y)$  matrix is transformed also, and arranged according to the same ordering indices of  $I$ . The two arrays define the function  $\rho(I)$ , which holds for the time  $t$ . Collecting the  $\rho(I)$  at all times, one obtains the complete response function of the system  $\rho(I,t)$ . This procedure is equivalent to a large number ( $40 \times 40$ ) of simultaneous measurements of the local retardation kinetics at different pump irradiance levels.

### 3. RESULTS

In Fig. 2 we report the absorption spectra of the samples. The absorbance peak for DR1 containing samples is at about 491 nm, whereas for DO3 it is at about 437 nm. While the peak position is determined by the dye, the absorption intensity depends on the presence and type of surfactants. For both groups, the absorption increases with the presence of the surfactants with SDS causing the highest effect. The spectrum of the sample A3 (PMMA:DR1:SDS) shows a quite flat structure. A similar behavior, even if less marked, may be noticed for sample B3 (PMMA:DO3:SDS). We have of course verified that the flatness of the absorption spectrum is not due to instru-

mental saturation; at least three close bands may be identified by a Gaussian deconvolution.

All the samples have been analyzed with the IPP setup. Figure 3 shows the retardation kinetics  $\rho(t)$  corresponding to the area element ( $57 \mu\text{m} \times 57 \mu\text{m}$ ) irradiated with the maximum irradiance level (about  $1.2 \text{ mW/mm}^2$ ). The highest values are obtained for DR1-based samples. For both dyes, the maximum retardation is obtained with SDS and the minimum is obtained for the nonmesostructured samples.

The retardation as a function of the local irradiance,  $\rho(I)$ , obtained at  $t_{\text{MAX}}$  is reported in Fig. 4 for each sample. The  $\rho(I)$  curves shown here differ from those usually reported in literature [16] as they have been obtained in a single experiment on a quasi-continuous range of irradiances. The six curves have the same exponential shape; this shape is observed at all times, both during growth and relaxation of the retardation (data not shown).

Following [10], we define the fractional residual retardation  $R = 100 \times \rho_{\text{LAST}}(I) / \rho_{\text{MAX}}(I)$ , where  $\rho_{\text{LAST}}$  is the retardation at the end of the relaxation ( $t_{\text{LAST}}$ ) and  $\rho_{\text{MAX}}$  is the maximum value (at  $t_{\text{MAX}}$ ) obtained at each irradiance value. The ratio  $R$ , shown in Fig. 5, measures the residual “memory” of the sample after a given relaxation time for a large range of excitation irradiances.

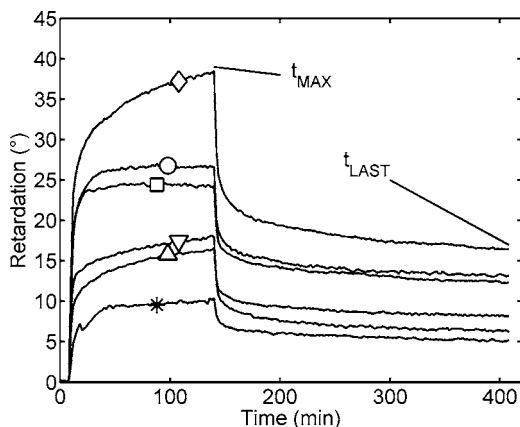


Fig. 3. Photoinduced retardation curves  $\rho(t)$  for the area element corresponding to the maximum pump irradiance in different samples. A1,  $\square$ ; A2,  $\circ$ ; A3,  $\diamond$ ; B1,  $*$ ; B2,  $\triangle$ ; B3,  $\nabla$ .

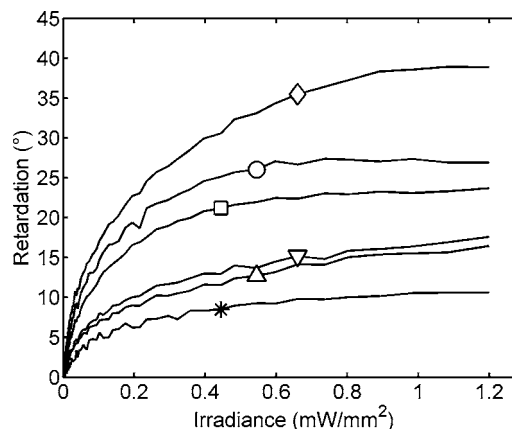


Fig. 4. Retardation-irradiance curves  $\rho(I)$  measured at the time  $t_{\text{MAX}}$  for each sample. A1,  $\square$ ; A2,  $\circ$ ; A3,  $\diamond$ ; B1,  $*$ ; B2,  $\triangle$ ; B3,  $\nabla$ .

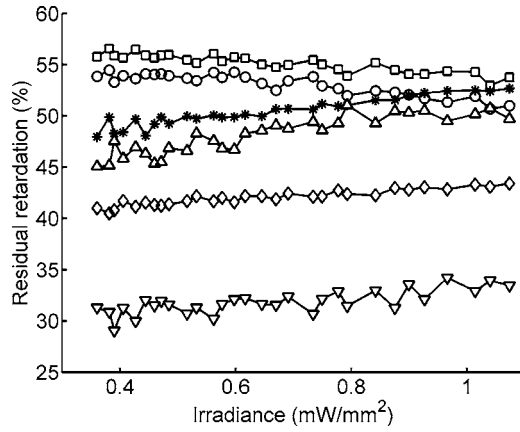


Fig. 5. Residual retardation as a function of the local irradiance. A1,  $\square$ ; A2,  $\circ$ ; A3,  $\diamond$ ; B1,  $*$ ; B2,  $\triangle$ ; B3,  $\nabla$ . Points calculated at low irradiance values have not been plotted due to high noise.

The ratio  $R$  is nearly constant at all the irradiance levels for each sample, in agreement with what was found in [10] for a hybrid sol-gel sample. On the other hand, our data show that  $R$  strongly depends on the chromophore type and the host structure. For both dyes, the minimum

**Table 2. Analytical Expressions for the PIB as a Function of Irradiance  $I$  at the Fixed Time  $t_{\text{MAX}}$  used in the Text for the Fitting of these Data**

Model	$\rho(I, t_{\text{MAX}})$
Monoexp [10]	$a_1[1 - \exp(-a_2I)]$
Sekkat and Knoll [14]	$a_1[\exp(-a_2It_{\text{MAX}}) - \exp(-a_3It_{\text{MAX}})]$
Sajti <i>et al.</i> [15]	$a_1I/[1 + t_{\text{MAX}}(a_2 + a_3I)]$
Thieghi <i>et al.</i> [16]	$a_1[1 - a_2/(a_2 + a_3I)]$ $\times \{1 - \exp[-(a_2 + a_3I)t_{\text{MAX}}]\}$ $[a_1a_2I/(a_2I + a_3)][a_4/(a_4 + a_5I + a_6)]$
Fu <i>et al.</i> [17]	$\times \{1 - \exp[-(a_2I + a_3)t_{\text{MAX}}]\}$ $\times \{1 + [(a_5I + a_6)/a_4]$ $\times \exp[-(a_4 + a_5I + a_6)t_{\text{MAX}}]\}$
Biexp	$a_1[1 - \exp(-a_2I)] + a_3[1 - \exp(-a_4I)]$

residual retardation is obtained in SDS-based systems and is maximum for the nonmesostructured (amorphous) ones.

Irradiance-retardation data measured at  $t_{\text{MAX}}$  have been fitted with the  $\rho(I)$  analytical curves obtained from the available models [15–17], whose expressions are reported in Table 2. Here, we consider also two other simple functions: the monoexponential [10] and the biexponential. The monoexponential is attractive for its simplicity. The biexponential function is universally known and applied in literature to describe retardation behavior *in time*, both during buildup and relaxation of the PIB. Its two characteristic times are usually attributed to distinct molecular mechanisms: angular hole burning and angular redistribution [8]. In this paper, we use a biexponential as a descriptive function of the retardation dependence on irradiance. Sekkat and Knoll’s model [14] is very similar to a biexponential *both in time and irradiance* as the product  $t$  by  $I$  appears at the exponents but the weights of its two components are not independent as in the “dummy” biexponential (see the expressions of the functions in Table 2).

Table 3 reports the residual sum of squares (RSS) and the coefficient of determination,  $R^2$ , obtained for each fitting function. The last column in Table 3 contains the values averaged over the six  $\rho(I)$  curves. Notably, the number of free parameters is different for each function of Table 2. It is interesting to notice that the models [15] and [16] give very similar fitting results (differences are found beyond the fourth decimal place of RSS and  $R^2$  values) as the model in [16] for the calculated values of the fitting parameters is analytically equivalent to that in [15].

#### 4. DISCUSSION

The absorption spectra indicate that the concentration of the dye is higher inside mesostructured samples than in amorphous ones, being maximum for lamellar systems (SDS), where the additional bands of the spectrum may be due to dye aggregation [19]. This agrees with photoconductivity studies [20], which suggest a larger amount of dye molecules between the planes of the lamellar system than within the tubes in the hexagonal mesostructures.

**Table 3. RSS and Coefficient of Determination ( $R^2$ ) Obtained by Fitting the  $\rho(I)$  Experimental Data at  $t_{\text{MAX}}$  with Different Analytical Models**

Model		A1	A2	A3	B1	B2	B3	Avg.
Monoexp [10]	RSS	0.707	1.532	4.493	0.176	0.883	0.651	1.407
	$R^2$	0.989	0.982	0.967	0.984	0.958	0.976	0.976
Sekkat and Knoll [14]	RSS	0.346	0.873	1.438	0.087	0.2	0.176	0.520
	$R^2$	0.995	0.99	0.99	0.992	0.991	0.993	0.992
Sajti <i>et al.</i> [15]	RSS	0.143	0.454	1.815	0.068	0.39	0.227	0.516
	$R^2$	0.998	0.995	0.987	0.994	0.982	0.991	0.991
Thieghi <i>et al.</i> [16]	RSS	0.143	0.454	1.815	0.068	0.39	0.227	0.516
	$R^2$	0.998	0.995	0.987	0.994	0.982	0.991	0.991
Fu <i>et al.</i> [17]	RSS	0.135	0.404	0.644	0.06	0.108	0.104	0.242
	$R^2$	0.998	0.995	0.995	0.995	0.995	0.996	0.996
Biexp	RSS	0.084	0.205	0.138	0.054	0.063	0.088	0.105
	$R^2$	0.999	0.998	0.999	0.995	0.997	0.997	0.997

The planes are spaced enough (about 4 nm) to allow a favorable arrangement of the molecules while the width of the tubes is almost half (2.2 nm) the plane spacing.

Our data show that the PIB from lamellar mesostructured systems (SDS) is stronger than that from hexagonal systems (CTAB), whereas the amorphous systems give the lowest response. Thus, the experiments reveal a correlation between the presence of mesostructures and the birefringence efficiency. This agrees for example with the higher birefringence induced in Langmuir–Blodgett azopolymeric films as compared to amorphous systems, which has been attributed to the organized nature of the samples [21]. However, this correlation is still unclear as the high birefringence could be due directly to the effect of the concentration, or indirectly to a chromophore–chromophore interaction (aggregation) or a chromophore–environment interaction inside the mesostructures during the photo-orientation.

Furthermore, the PIB in our mesostructured samples has a lower residual retardation. To explain this, we can suppose a “restoring” effect due to the interaction of the chromophores with the hosting mesostructures. In dark conditions (before the irradiation), the dye molecules are packed inside the mesostructure, forming a molecular assembly that can be tubular or planar due to the influence of the cavity walls. The assemblies are distributed isotropically because the mesocavities are distributed randomly inside the matrix, and then the system is optically isotropic at the macroscopic level. During the irradiation, the dye molecules are forced to assume a macroscopic anisotropic distribution, but when the light is off, they reorientate according to the local configuration of the mesocavity. In contrast, in the amorphous systems, the only restoring mechanism is the thermal reorientation. An additional explanation of the high efficiency and low relaxation time could be a large free volume for the dye molecules in the mesostructured samples, enabling easier chromophores orientation and back reorientation.

The theoretical models applied to fit these  $\rho(I)$  data gave different fitting results. The worst model is the monoexponential (RSS=1.407,  $R^2=0.976$ ) while the better one is the biexponential (RSS=0.105,  $R^2=0.997$ ). The latter is a phenomenological model and would suggest two mechanisms responsible for the PIB with characteristic irradiance levels  $1/a_2$  and  $1/a_4$ , respectively. Our experimental approach makes available the continuous curves  $\rho(I)$ , thanks to the imaging birefringence technique and its point-to-point correlation between retardation maps and irradiance maps. This makes the difference with the usual description of the kinetics of the PIB, in which the retardation is considered at a fixed intensity as a function of time.

In regard to the other models, it is very interesting to notice that, neglecting the Fu *et al.* model [17], which requires a high number of free parameters, the other physical models (Sekkat and Knoll [14], Sajiti *et al.* [15], and Thieghi *et al.* [16]) give similar results. At last, our results show that all observations made here about the effects of mesostructures apply both to DR1- and DO3-based samples. The only apparent differences are the efficiency of the PIB phenomenon and its residue value, which are

mainly due to the different absorption coefficient values of the two molecules at the wavelength of the pump light.

## 5. CONCLUSIONS

Spectroscopic and imaging pump-probe analyses show that the mesostructured nature of the samples has a remarkable influence on their properties. The templating surfactants CTAB and SDS allow the highest concentration of dye molecules, which probably fill the tubular or lamellar mesostructures. The imaging pump-probe technique enables the measurement of the retardation-irradiance curves that may be fitted with current models. Mesostructured samples give the strongest birefringence signal. The residual birefringence in mesostructured samples is lower than in amorphous ones due to the interaction of chromophores with the hosting mesostructures.

## REFERENCES

1. V. Zucolotto, C. R. Mendonça, D. S. dos Santos, D. T. Balogh, S. C. Zilio, O. N. Oliveira, Jr., C. J. L. Constantino, and R. F. Aroca, “The influence of electrostatic and *H*-bonding interactions on the optical storage of layer-by-layer films of an azopolymer,” *Polymer* **43**, 4645–4650 (2002).
2. C. R. Mendonça, D. S. dos Santos, Jr., D. T. Balogh, A. Dhanabalan, J. A. Giacometti, S. C. Zilio, and O. N. Oliveira, Jr., “Optical storage in mixed Langmuir–Blodgett (LB) films of azopolymers and cadmium stearate,” *Polymer* **42**, 6539–6544 (2001).
3. Y. Wu, Q. Zhang, A. Kanazawa, T. Shiono, T. Ikeda, and Y. Nagase, “Photoinduced alignment of polymer liquid crystals containing azobenzene moieties in the side chain 5. effect of the azo contents on alignment behavior and enhanced response,” *Macromolecules* **32**, 3951–3956 (1999).
4. H.-K. Lee, K. Doi, H. Harada, O. Tsutsumi, A. Kanazawa, T. Shiono, and T. Ikeda, “Photochemical modulation of color and transmittance in chiral nematic liquid crystal containing an azobenzene as a photosensitive chromophore,” *J. Phys. Chem. B* **104**, 7023–7028 (2000).
5. O. N. Oliveira, Jr., S. Yang, V. Zucolotto, J. A. He, C. J. L. Constantino, A. L. Cholli, L. Li, R. F. Aroca, J. Kumar, and S. K. Tripathy, “Surface relief gratings on azobenzene-containing films. Mechanism and recent developments,” *Mol. Cryst. Liq. Cryst. Sci. Technol., Sect. A* **374**, 67–76 (2002).
6. C. J. L. Constantino, R. F. Aroca, J. A. He, V. Zucolotto, L. Li, O. N. Oliveira, Jr., J. Kumar, and S. K. Tripathy, “Raman microscopy and mapping as a probe for photodegradation in surface relief gratings recorded on layer-by-layer films of congo red/polyelectrolyte,” *Appl. Spectrosc.* **56**, 187–191 (2002).
7. Y. L. Wu, A. Natansohn, and P. Rochon, “Photoinduced birefringence and surface relief gratings in novel polyurethanes with azobenzene groups in the main chain,” *Macromolecules* **34**, 7822–7828 (2001).
8. I.-G. Marino, D. Bersani, and P. P. Lottici, “Photoinduced birefringence in DR1 doped sol-gel silica and ORMOSILs thin films,” *Opt. Mater.* **15**, 175–180 (2000).
9. I.-G. Marino, C. Razzetti, and P. P. Lottici, “Wide-field polarimetric analysis of photoinduced birefringence in azo-dye-doped thin films: irradiance and time dependence,” *Appl. Phys. B: Lasers Opt.* **86**, 687–672 (2007).
10. I.-G. Marino, C. Razzetti, P. P. Lottici, and F. Nazzari, “An investigation of photoinduced birefringence in disperse red 1-polymethylmethacrylate films by polariscopic imaging,” *Thin Solid Films* **516**, 8462–8467 (2008).

11. M. Huang, F. Kartono, B. Dunn, J. Zink, G. Valverde, and J. García, "Hexagonal to lamellar mesostructural changes in silicate films caused by organic additives," *Chem. Mater.* **14**, 5153–5162 (2002).
12. A. Franco, V. Rentería, G. Valverde-Aguilar, J. A. García-Macedo, "Photoconductivity for silver nitrate in nanostructured sol-gel materials," *J. Nanosci. Nanotechnol.* **8**, 1–7 (2008).
13. C. E. Fowler, B. Lebeau, and S. Mann, "Covalent coupling of an organic chromophore into functionalized MCM-41 mesophases by template-directed co-condensation," *Chem. Commun.* 1825–1826 (1998).
14. Z. Sekkat and W. Knoll, "Creation of second-order nonlinear optical effects by photoisomerization of polar azo dyes in polymeric films: theoretical study of steady-state and transient properties," *J. Opt. Soc. Am. B* **12**, 1855–1867 (1995).
15. S. Sajti, Á. Kerekes, P. S. Ramanujam, and E. Lórinicz, "Response function for the characterization of photo-induced anisotropy in azobenzene containing polymers," *Appl. Phys. B: Lasers Opt.* **75**, 677–685 (2002).
16. L. T. Thieghi, F. Batalioto, I. H. Bechtold, L. R. Evangelista, V. Zucolotto, D. T. Balogh, O. N. Oliveira, Jr., and E. A. Oliveira, "Phenomenological analysis of the light intensity dependence of the photoalignment process in azo-containing polymeric films," *Phys. Rev. E* **74**, 011802 (2006).
17. S. Fu, W. Hu, M. Xie, G. Wang, Y. Li, Q. Duanmu, J. Tian, and Y. Liu, "A new kinetic description of the complex optical behavior in photochromic polymer films," *Physica B* **400**, 198–202 (2007).
18. J. García-Macedo, G. Valverde, D. Cruz, A. Franco, J. I. Zink, and P. Minoofar, "Structure and polyphenylvinylene concentration effect on the photoconductivity response from mesostructured silica films," *J. Phys. Chem. B* **107**, 2249–2252 (2003).
19. E. Rivera, M. P. Carreón-Castro, I. Buendía, and G. Cedillo, "Optical properties and aggregation of novel azo-dyes bearing an end-capped oligo(ethylene glycol) side chain in solution, solid state and Langmuir-Blodgett films," *Dyes Pigm.* **68**, 217–226 (2006).
20. G. Valverde, J. García-Macedo, D. Cruz, J. I. Zink, and R. Hernández, "Photoconductivity in mesostructured thin films," *J. Sol-Gel Sci. Technol.* **26**, 605–608 (2003).
21. O. N. Oliveira, Jr., D. S. dos Santos, Jr., D. T. Balogh, V. Zucolotto, and C. R. Mendonça, "Optical storage and surface-relief gratings in azobenzene-containing nanostructured films," *Adv. Colloid Interface Sci.* **116**, 179–192 (2005).